IEEE Access
Multidisciplinary | Rapid Review | Open Access Journal

Received December 3, 2019, accepted January 28, 2020, date of publication February 3, 2020, date of current version February 11, 2020.

Digital Object Identifier 10.1109/ACCESS.2020.2971107

Experimental Research on Lightning Disturbance Characteristics of 10-kV Fusion Voltage Transformer Intelligent Component Acquisition Port

QI WANG, ZIHAN TENG, FANWU CHU, YUE TONG, JUNJUN XIONG, GUOXIONG YE, AND XIONG WU

China Electric Power Research Institute, Wuhan 430074, China

Corresponding author: Qi Wang (373201386@qq.com)

This work was supported in part by the National Natural Science Foundation of China under Grant U1866201, and in part by the Natural Science Foundation of Hubei Province under Grant 2018CFB189.

ABSTRACT In the lightning impulse test, the 10 kV fusion voltage transformer intelligent component acquisition port often suffers from functional failure or breakdown. In this paper, experimental measurement and inversion calculation were used to study the electromagnetic disturbance level of smart component acquisition port. During the inversion calculation, the applicability of the dual exponential function model, Heidler function model, and impulse function model as the primary source for describing the lightning impulse device were compared and analyzed. The results show that the double exponential model was used as the calculation source of the primary side lightning waveform, and the inversion calculation results were in good agreement with the actual measurement. In addition, the effects of the primary side lightning voltage peak, wave head, and wave tail parameters on the maximum amplitude of the disturbance waveform calculated by inversion are discussed and analyzed. Based on the analysis results, a sufficient inversion calculation parameter was proposed to estimate the disturbance level of the intelligent component acquisition port. Finally, the measured results were compared and discussed with the IEC 61439 assessment level, and it was suggested that the assessment level of fusion equipment should be modified.

INDEX TERMS Electromagnetic interference (EMI), lightning impact test, inversion calculation, port disturbance voltage, smart component, lightning model.

I. INTRODUCTION

With the development of distribution network automation technology, a large number of fusion type voltage transformer signal acquisition equipment with intelligent sensing, judgment and execution functions are applied to distribution network lines [1]. Lightning impulse test is one of the items of factory type test. It is used to assess the ability of the main insulation of voltage transformers and intelligent components to withstand the impact voltage. According to the data from the production department, under the lightning impulse test, the secondary equipment in the intelligent component often misoperates or is damaged, and the failure of the data acquisition unit accounts for a large proportion [2]. Therefore, it is urgent to master the disturbance level of the transient disturbance voltage coupled to the signal acquisition port of intelligent components under the standard lightning voltage assessment, on this basis, effective protection measures are formulated.

Many experimental measurement and calculation methods were used to study the impact of lightning power transient signals on secondary equipment. The United States Electric Power Research Institute (EPRI) had reported a large number of electromagnetic interference levels of secondary electronic equipment in the case of air insulated switchgear (AIS) and gas insulated switchgear (GIS) substations including lightning strikes, short circuits, and switching operations since the last century [3]. Matveyev *et al.* Measured and analyzed

The associate editor coordinating the review of this manuscript and approving it for publication was Mehmet Alper Uslu.

the interference caused by the transient ground potential rise and the transient ground potential difference to the secondary system caused by lightning stroke in the substation [4]. On the basis of the experiments, the Chen's team studied the influence of the spatial magnetic field disturbance caused by the current under the impact of lightning on smart components, and proposed the level requirements for immunity level [5], [6].

At the same time, there were corresponding international guidelines and standards for primary and secondary equipment, including test methods, test assessment level, etc. [7]–[9]. However, these studies mostly focused on traditional equipment and application environments. At that time, this new application situation of decentralized intelligent secondary equipment was less involved. Under the new situation, the actual disturbance level of intelligent component acquisition port under the lightning voltage test has not been extensively demonstrated. In this paper, based on the broadband transmission characteristics of voltage transformer, different lightning mathematical models were used for inversion calculation. The experimental results showed that the maximum disturbance level calculated by the double exponential model was in good agreement with the actual measurement results. At the same time, the influence of the maximum amplitude U_0, wave head parameter t_1, and wave tail parameter t_2 in the standard range on the maximum amplitude of the inversion calculation were discussed and analyzed, and the universal inversion calculation parameters were proposed.

This paper is organized as follows. Section II introduces the structural characteristics and inverse calculation model of the fusion voltage transformer equipment. Section III describes the calculation results obtained by inversion calculation of the source function and different lightning model functions. And the calculation results are compared and analyzed with the experimental measured results. Section IV discusses the influence of the maximum amplitude U_0, wave head parameter t_1, and wave tail parameter t_2 within the standard range on the maximum amplitude of the inversion calculation. Finally, this paper is summarized in Section V.

II. EQUIPMENT STRUCTURE AND CALCULATION MODEL

A. EQUIPMENT STRUCTURAL CHARACTERISTICS

The voltage dividing principle of voltage transformer fusion equipment mainly includes three types: electromagnetic, capacitive and resistance-capacitance. According to the degree of fusion, it is mainly divided into two types: complete equipment and integrated integration equipment. Their common feature is that the traditional primary equipment and secondary control intelligent unit are combined and installed locally on the site. The secondary intelligent component integrates multiple functional modules such as automatic measurement and control protection, communication management, and power supply, etc. Compared with the traditional equipment with more than 100 meters long connection transmission cable, the fusion equipment has a shorter primary and secondary transmission distance. At present, the transmission cable length of complete equipment mainly includes 1 m, 3 m, 6 m, 8 m, 10 m, 15 m, etc., and the length of the transmission cable connected by the integrated equipment is closer to 0m. In addition, the secondary-side port power frequency measurement voltage is also reduced from $100/\sqrt{3}$ V to $3.5/\sqrt{3}$ V.

FIGURE 1. Typical fusion equipment application scenario diagram.

Figure 1 shows the typical application scenario of voltage transformer fusion equipment. This paper focuses on the disturbance level of acquisitional port in the marked part of the figure under the standard lightning impulse.

B. CALCULATION MODEL

There are two methods to obtain the actual disturbance level of the intelligent component acquisition port under the lightning assessment. The first is the actual measurement at the acquisition port during the lightning strike test. The second is to perform inversion calculations based on the disturbance waveform and transfer function.

In this paper, the black-box principle is used to establish a two-port transfer function calculation model for an unknown system in the frequency domain as shown in Figure 2. This model can measure the voltage time-domain waveforms $U_1(t)$ and $U_2(t)$ on the primary side and the intelligent component acquisition port by using the low level lightning pulse. $U_1(t)$, $U_2(t)$ fast Fourier transform can obtain corresponding frequency domain signals U_1 (jω), U_2(jω). Let A(jω), B(jω), C(jω), D(jω) be the transmission parameters of an unknown system, then the frequency domain transmission T of the system can be expressed as a matrix (1).

$$T = \begin{bmatrix} A(\mathrm{j}\omega) & B(\mathrm{j}\omega) \\ C(\mathrm{j}\omega) & D(\mathrm{j}\omega) \end{bmatrix} \tag{1}$$

According to the transmission characteristics, equation 2 can be obtained.

$$U_1(\mathrm{j}\omega) = A(\mathrm{j}\omega)U_2(\mathrm{j}\omega) + B(\mathrm{j}\omega)I_2(\mathrm{j}\omega) \tag{2}$$

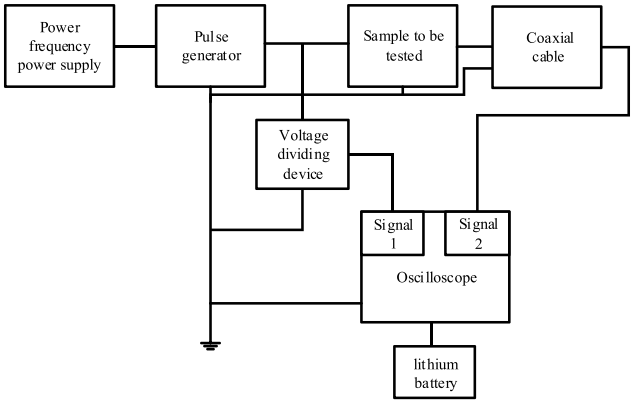

FIGURE 2. Transfer characteristic measurement test circuit diagram.

In engineering, in order to ensure the accuracy of measurement data at power frequency, the input impedance of the data acquisition card is usually very large. For example, China's T/CES 033-2019 related standards suggest that the input impedance should be greater than 5 MΩ [23]. Therefore, the input current of the intelligent component acquisition port is very small, and $I_2(\mathrm{j}\omega) \approx 0$ can be set.

Equation (2) can be reduced to equation (3).

$$U_1(\mathrm{j}\omega) = A(\mathrm{j}\omega)U_2(\mathrm{j}\omega) \tag{3}$$

So the reciprocal $E(\mathrm{j}\omega)$ of $A(\mathrm{j}\omega)$ is equation (4).

$$E(\mathrm{j}\omega) = U_2(\mathrm{j}\omega)/U_1(\mathrm{j}\omega) \tag{4}$$

If the primary side frequency domain characteristic function U_3 (jω) is known during the lightning impulse test, the frequency domain U_4 (jω) of the secondary side waveform can be obtained by convolution calculation of E (jω) and U_3 (jω). The calculation formula is shown in Equation (5).

$$U_4(\mathrm{j}\omega) = E(\mathrm{j}\omega)U_3(\mathrm{j}\omega) \tag{5}$$

The time domain voltage signal waveform $U_4(t)$ of the intelligent component acquisition port can be obtained by performing discrete Fourier inverse transform on U_4(jω)

III. ANALYSIS OF MEASUREMENT AND INVERSION CALCULATION RESULTS

A. COMPARATIVE ANALYSIS OF MEASURED DATA AND SOURCE FUNCTION INVERSION

In order to verify the validity of the calculation model, eight voltage transformer fusion devices numbered ①–⑧ were selected in the laboratory for the secondary side acquisition port measurement under lightning impulse test. At the same time, the frequency-domain transfer function $E(\mathrm{j}\omega)$ of these 8 devices was obtained by using the pulse generator device under the lightning pulse with low amplitude (±4 kV). During the test, the oscilloscope port connected on the primary side was selected for 50 Ω matching. The secondary port was disconnected from the intelligent component and selected for 1 M Ω matching.

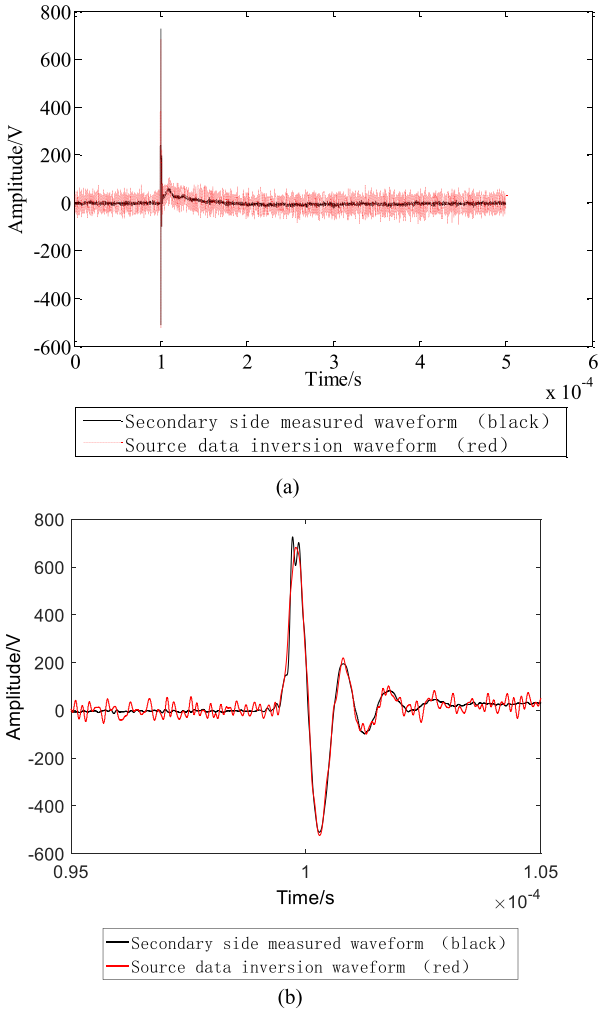

FIGURE 3. (a) Full-time domain diagram of measured waveform and inverse calculated waveform on the secondary side of sample ①. (b) Partial time-domain expanded view of the measured waveform and inverse calculated waveform on the secondary side of sample①.

There were compared and analyzed the waveform obtained from the inversion of the primary source data and the measured waveform of the secondary side. It can be found that the measured waveforms of each sample are similar to the inversion calculated waveforms in general. Select the full time-domain waveform and local time-domain waveform of sample ① as representative displays, as shown in Figures 3(a) and 3(b).

It can be seen from Figs. 3(a) and 3(b) that the calculated waveform has numerical oscillations, and the overall inversion waveform is generally consistent with the measured waveform. In the electromagnetic disturbance, protection and test assessment, more attention is paid to the maximum disturbance voltage of the disturbance waveform. The error rate ε of formula (6) is used to evaluate the error of the maximum disturbance voltage.

$$\varepsilon = \frac{\max\left|U_i'\right| - \max|U_i|}{\max|U_i|} \times 100\% \tag{6}$$

where U_i is the measured voltage data point and U_i' is the calculated voltage data point.

The ε in Figure 3 is -6.07%, which is acceptable in engineering. Therefore, it can be considered that the maximum disturbance voltage of the secondary-side acquisition port obtained by the actual measurement and source function inversion calculation is equivalent.

B. INVERSION OF DIFFERENT LIGHTNING MATHEMATICAL MODELS

Both methods in III-A need to obtain relevant data under full voltage lightning wave assessment. However, the lightning impulse test is a destructive insulation test. It may cause damage to the main equipment to obtain the maximum disturbance voltage distribution of the secondary side by repeatedly conducting full voltage lightning wave test on the main equipment according to the standard. In order to reduce this risk, the primary-side source data needed for inversion calculation can be considered using existing lightning mathematical models to describe. At present, double exponential function model [10], Heidler function model [11] and impulse function model [12] are more commonly used and recommended.

The mathematical equation of the double exponential function model is expressed as equation (7).

$$F_1(t) = \mu_1 U_0 \left(e^{-t/\tau_2} - e^{-t/\tau_1}\right) \tag{7}$$

Heidler function model mathematical equation expression is equation (8).

$$F_2(t) = \mu_2 U_0 \frac{(t/\tau_1)^n}{1 + (t/\tau_1)^n} e^{-t/\tau_2} \tag{8}$$

The mathematical equation of the impulse function model is expressed as equation (9).

$$F_3(t) = \mu_3 U_0 \left(1 - e^{-t/\tau_1}\right) e^{-t/\tau_2} \tag{9}$$

where U_0 is the peak value of lightning voltage. μ_1, μ_2, and μ_3 are the wave calibration coefficients. τ_1 is the wave head attenuation coefficient. τ_2 is the wave tail attenuation coefficient. n is the steepness factor, generally n=2 or n=10. Among them, the calculation of the coefficients μ_2 and μ_3 can be found in equations (10) and (11).

$$\mu_2 = 1/\exp\left[-\frac{\tau_1}{\tau_2}\left(n\frac{\tau_2}{\tau_1}\right)^{1/n}\right] \tag{10}$$

$$\mu_3 = 1/\left[\left(1 - \frac{\tau_1}{\tau_1 + n\tau_2}\right)^n \left(\frac{\tau_1}{\tau_1 + n\tau_2}\right)^{\tau_1/\tau_2}\right] \tag{11}$$

According to the definition of the lightning waveform, the simultaneous solving equations can obtain the values of $\mu_1, \mu_2, \mu_3, \tau_1, \tau_2$ corresponding to different wavefront times t_1 and half-peak times t_2. After comparing the maximum amplitudes of the disturbance waveforms measured on the secondary side of the eight samples, samples ①, ④, and ⑤ were selected as typical samples. Take $n = 10$, Table 1 corresponds to the values of μ_1, μ_2, μ_3, τ_1, τ_2 at U_0, t_1, and t_2,

TABLE 1. Parameter value corresponding to the standard deviation boundary waveform.

Sample number	Primary side t_1/t_2 (μs)	μ_1	μ_2	μ_3	τ_1 (μs)	τ_2 (μs)
①	1.15/52.4	1.034	1.011	1.047	0.386	71.81
④	1.42/47.8	1.046	1.012	1.064	0.488	64.42
⑤	1.05/51.2	1.032	1.011	1.044	0.351	70.38

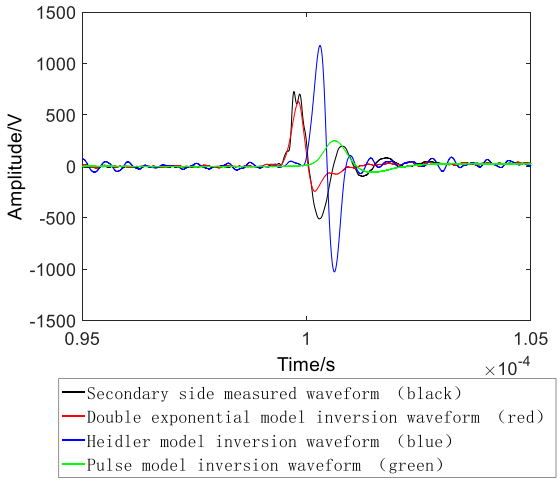

FIGURE 4. Partially expanded view of the measured waveform and inverse calculated waveform on the secondary side of sample ①.

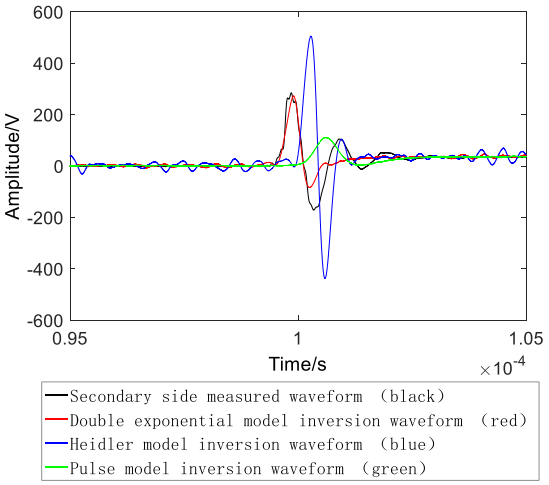

FIGURE 5. Partially expanded view of the measured waveform and inverse calculated waveform on the secondary side of sample ④.

which are the same as the primary side power supply waveform of the equipment under test ①, ④, ⑤.

The overall time-domain diagram of the secondary side waveforms calculated under the three lightning mathematical models is similar to Figure 3 (a). In order to facilitate the observation and analysis, the partial expanded views near the peaks are shown in Figs. 4, 5, and 6.

It can be seen from figure 4-6 that there are differences between the inversion calculation waveform and the measured waveform of the three lightning mathematical models,

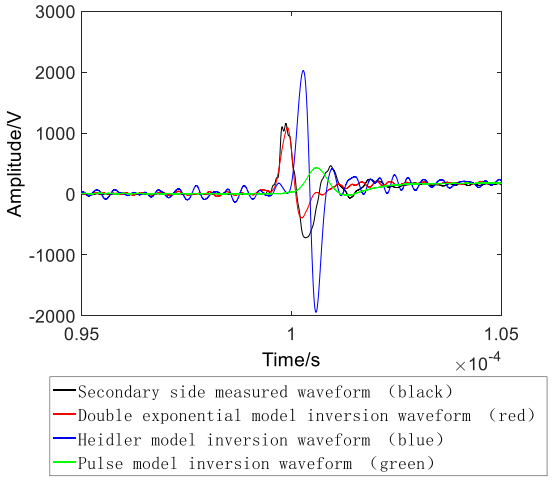

FIGURE 6. Partially expanded view of the measured waveform and inverse calculated waveform on the secondary side of sample ⑤.

among which the calculation results of the Heidler function model and the pulse function model are greatly different. According to equation (6), the maximum disturbance voltage amplitude of the point of interest is compared. The deviation rate of the double exponential model is $(-13.50 \sim -4.04)$ %, the deviation rate of the Heidler function model is $(+61.71 \sim +77.31)$ %; the deviation rate of the pulse function model is $(-65.65 \sim -61.01)$ %. In terms of deviation rate, the inversion calculation using the double exponential model is more consistent with the actual measurement results. In addition, in the IEC61000-4 series of standards, there is a significant difference in the assessment amplitudes for different levels of immunity, and errors within 13.50% do not prevent us from accurately selecting the assessment level [7]–[9]. Therefore, this error is acceptable in engineering applications, and the double exponential model can be used as the source function of the primary side lightning wave for inversion calculation.

IV. DISCUSSION AND ANALYSIS

A. ANALYSIS OF INFLUENCE OF LIGHTNING PARAMETERS ON INVERSION

In fact, the actual primary waveform parameters U_0, t_1 and t_2 are unknown. During the test, it is randomly distributed within the allowable range of standard deviation. Taking 10 kV voltage level as an example, the peak value of the lightning full wave U_0 is 75 ($\pm$3%) kV, the wave head time t_1 is 1.2 ($\pm$30%) μs, and the half-peak time t_2 is 50 ($\pm$20%) μs. This section mainly discusses the influence of U_0, t_1 and t_2 changes within the standard range on the maximum amplitude of the inversion calculation.

In Section III, it has been demonstrated that when the relevant parameters of the dual exponential function model match U_0, t_1 and t_2, the results of the inversion calculation are in good agreement with the actual measurement. Therefore, the influence of analysis parameter changes on the inversion calculation can be discussed mathematically through the double exponential function model.

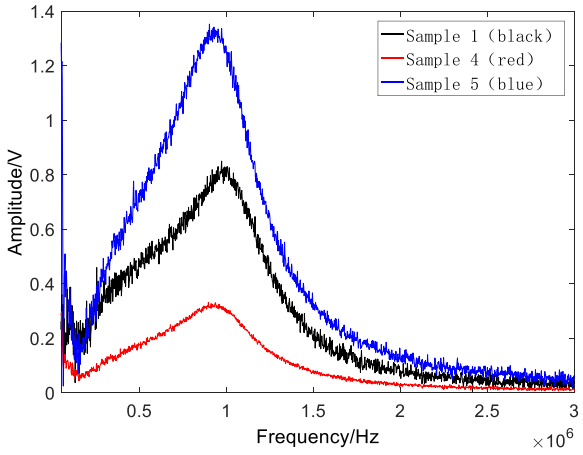

FIGURE 7. Frequency domain diagram of the measured waveform on the secondary side of samples ①, ④, and ⑤.

Fourier transform the equation (6), and its frequency domain is equation (12).

$$F_1(j\omega) = \mu_1 U_0 \left(\frac{1}{\tau_2 + j\omega} - \frac{1}{\tau_1 + j\omega} \right) \tag{12}$$

For a fixed voltage transformer fusion device, its $E(j\omega)$ is a constant value. When t_1 and t_2 are the same, μ_1, τ_1 and τ_2 are the same. Obviously, the quadratic waveform calculated according to the inversions of equations (5) and (12) has a positive correlation with U_0.

In order to analyze the effects of t_1 and t_2 under the same U_0, equation (13) is obtained by normalizing equation(12).

$$G(j\omega) = \mu_1 \left(\frac{1}{1/\tau_2 + j\omega} - \frac{1}{1/\tau_1 + j\omega} \right) \tag{13}$$

According to equation (13), the amplitude-frequency characteristic equation (14) and the phase-frequency characteristic equation (15) can be obtained.

$$|G(j\omega)| = \frac{\mu_1 \sqrt{\left[\omega^4 + \left(\frac{\omega}{\tau_1}\right)^2 + \left(\frac{\omega}{\tau_2}\right)^2 + \left(\frac{1}{\tau_1\tau_2}\right)^2\right]\left(\frac{1}{\tau_2} - \frac{1}{\tau_1}\right)^2}}{\left[\left(\frac{1}{\tau_1}\right)^2 + \omega^2\right]\left[\left(\frac{1}{\tau_2}\right)^2 + \omega^2\right]} \tag{14}$$

$$\theta(\omega) = arctan\left[\frac{\omega\left(\frac{1}{\tau_1} + \frac{1}{\tau_2}\right)}{\omega^2 - \frac{1}{\tau_1\tau_2}}\right] \tag{15}$$

The amplitude-frequency characteristics of the measured disturbance waveforms on the secondary-side of the samples ①, ④, and ⑤ are shown in Figure 7. As can be seen from the figure, the amount of disturbance is mainly concentrated in the 0.2-2.5 MHz frequency band. Therefore, it is mainly compared that the equations (14) and (15) in the 0.2-2.5 MHz frequency domain are affected by μ_1, τ_1 and τ_2.

In the 0.2-2.5 MHz frequency band, $\omega^2 = (2\pi f)^2$ is above the order of 10^{12}. Within the standard deviation range

TABLE 2. Parameter value corresponding to the standard deviation boundary waveform.

t_1/t_2 (μs)	μ_1	τ_1 (μs)	τ_2 (μs)
1.15/40.0	1.044	0.3937	54.02
1.15/60.0	1.030	0.3824	82.72
0.84/52.4	1.025	0.2765	72.74
1.56/52.4	1.046	0.5357	70.61
1.42/40.0	1.055	0.4957	53.24
1.42/60.0	1.037	0.4788	81.92
0.84/47.8	1.028	0.2779	66.13
1.56/47.8	1.050	0.5402	64.02
1.05/40.0	1.041	0.3568	54.31
1.05/60.0	1.028	0.3472	83.02
0.84/51.2	1.026	0.2768	71.02
1.56/51.2	1.047	0.5368	68.89

of 1.2/50 us, $\frac{1}{\tau_2}$ is within the order of 10^4, $\frac{1}{\tau_1}$ is in the order of 10^6, and $\frac{1}{\tau_1\tau_2}$ is in the order of 10^{10}.

Thus, equations (14) and (15) can be reduced to equations (16) and(17).

$$|G(j\omega)| \approx \frac{\mu_1\left(\frac{1}{\tau_1}-\frac{1}{\tau_2}\right)\sqrt{\omega^2\times\left[\omega^2+\left(\frac{1}{\tau_1}\right)^2+\left(\frac{1}{\tau_2}\right)^2\right]+\left(\frac{1}{\tau_1\tau_2}\right)^2}}{\omega^2\times\left[\left(\frac{1}{\tau_1}\right)^2+\omega^2\right]} \approx \frac{\mu_1\frac{1}{\tau_1}\sqrt{\omega^2\times\left[\omega^2+\left(\frac{1}{\tau_1}\right)^2\right]}}{\omega^2\times\left[\left(\frac{1}{\tau_1}\right)^2+\omega^2\right]} = \frac{\mu_1}{\omega\times\sqrt{(\omega\tau_1)^2+1}} \quad (16)$$

$$\theta(\omega) \approx \arctan\left(\frac{\omega\times\frac{1}{\tau_1}}{\omega^2}\right) = arctan\left(\frac{1}{\omega\tau_1}\right) \quad (17)$$

From equations (16) and (17), it can be known that in the 0.2-2.5 MHz frequency band, the amplitude-frequency characteristics and phase-frequency characteristics of the primary source within the standard deviation range are mainly affected by τ_1, while τ_2 has little influence. τ_1 is positively correlated with t_1, τ_2 is positively correlated with t_2, and the interaction of t_1 and t_2 slightly affects μ_1. Therefore, the smaller the t_1, the larger the amplitude of the disturbance $|G\ (j\omega)|$, the larger the maximum disturbance amplitude on the secondary side. The larger the t_1, the smaller the amplitude of the disturbance $|G\ (j\omega)|$, the smaller the secondary side. And t_2 has almost no influence on the maximum disturbance amplitude on the secondary side.

The above analysis was verified on samples ①, ④, ⑤. Table 2 is to keep one of t_1, and t_2 unchanged, and the other is

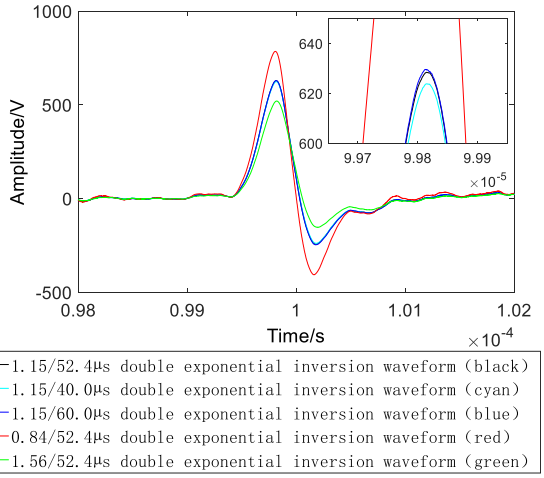

FIGURE 8. Partially developed secondary sample waveforms of sample ① with different parameters inversion.

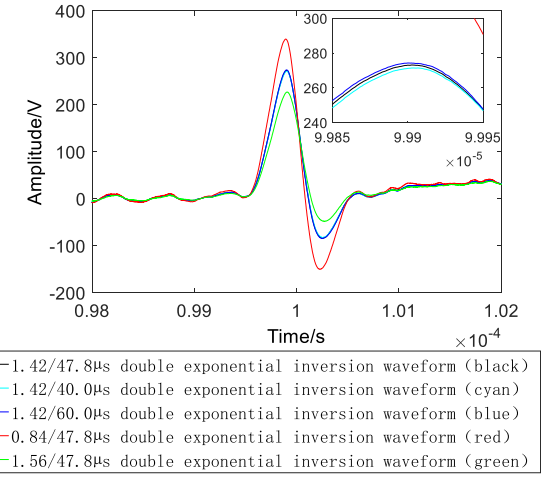

FIGURE 9. Partially developed secondary sample waveforms of sample ④ with different parameters inversion.

the corresponding μ_1, τ_1, τ_2 values at the standard deviation boundary value. The comparison results of the application of the double exponential model inversion under several deviation boundaries are shown in Fig. 8, Fig.9, and Fig. 10.

From Figure 8-10, it can be seen that under the same U_0, the double exponential function model is applied. When t_1 is maintained and only t_2 is changed, the black line, the blue line, and the cyan line basically coincide, so that it is almost impossible to distinguish them in the graph. While keeping t_2 unchanged and changing t_1, the inversion calculation waveform has obvious changes. And the smaller the t_1, the larger the maximum disturbance amplitude of the inversion waveform. The larger the t_1, the smaller the maximum disturbance amplitude of the inversion waveform. The time domain waveform inversion is consistent with the previous theoretical analysis. Therefore, 75 (+3%) kV, 0.84/50 (±20%) μs double exponential wave is selected as the primary source, combined with the transfer function obtained under low voltage pulse for inversion calculation and prediction. The maximum disturbance amplitude of the secondary port of the

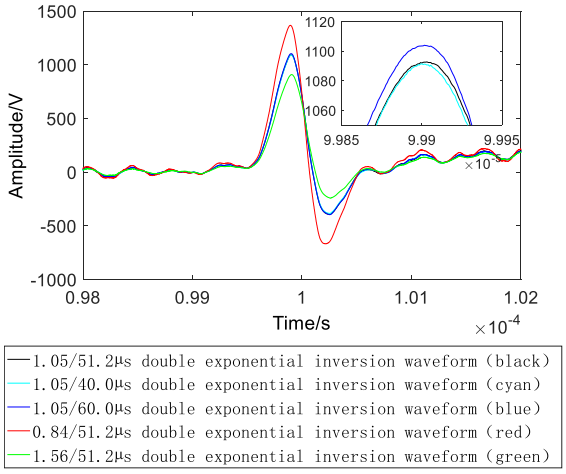

FIGURE 10. Partially developed secondary sample waveforms of sample ⑤ with different parameters inversion.

TABLE 3. Maximum disturbance voltage amplitude statistics.

Sample number	Measured disturbance voltage peak (V)	Inverse calculation of disturbance voltage peak (V)
①	726.6	781.9
②	833.0	916.4
③	35.8	41.5
④	284.7	339.1
⑤	1158.0	1359.0
⑥	210.7	224.3
⑦	868.5	990.8
⑧	1301.4	1402.6

fusion voltage transformer under the standard lightning wave assessment is sufficient.

B. SAMPLE MEASUREMENT AND INVERSION CALCULATION DATA

Table 3 shows the statistics of the measured maximum disturbance amplitude of eight samples under the standard lightning wave examination and the inversion calculation of the maximum disturbance voltage amplitude of the secondary side under 75 (+3%) kV and 0.84/50 μs by the double exponential function model.

The following conclusions can be drawn from table 3.

1) Under the standard lightning impulse test, the disturbance level of the acquisition port on the secondary intelligent component is far higher than the steady-state rated working voltage of $3.5/\sqrt{3}$ V, so it is necessary to consider the EMC protection measures of the acquisition port.
2) The maximum amplitude of the disturbance waveform of each device under the lightning shock test is quite different, and the maximum amplitude of some samples is higher than 1.0kV required by IEC 61439. Therefore, the existing secondary equipment standard assessment requirements do not match the primary equipment standard and should be considered for amendment.
3) The peak value of the measured disturbance voltage of the sample is basically smaller than the estimated value of the inversion calculation. Using the inversion calculation method summarized in this paper, the maximum amplitude of the disturbance of the secondary-side intelligent component acquisition port under the lightning assessment can be fully estimated.

V. CONCLUSION

The disturbance level of the intelligent component acquisition port of the 10 kV fusion voltage transformer under the lightning impulse test was measured and calculated. The conclusions are summarized as follows.

1) The comparison results show that it is equivalent to obtain the maximum disturbance voltage of the secondary-side acquisition port of the fusion voltage transformer by the two methods of actual measurement and source function inversion calculation.
2) Consider using the dual exponential function model, Heidler function model and impulse function model to replace the primary side source function. The inversion calculation results show that the dual exponential function model is used to describe the primary source waveform generated by the lightning impulse generator device. The calculated results are in good agreement with the measured results.
3) The influences of the maximum amplitude U_0, wave head parameter t_1, and wave tail parameter t_2 in the standard range on the maximum amplitude of the inversion calculation are discussed and analyzed. The results show that under the same t_1 and t_2 parameters, the maximum amplitude of the secondary waveform changes positively with U_0. Under the same U_0, the maximum amplitude of the secondary side calculated by the inversion is mainly affected by the wave head parameter t_1, and the effect of the wave tail parameter t_2 is small. The maximum disturbance amplitude increases with the decrease of t_1.On this basis, 75 (+3%) kV and 0.84/50 ($\pm$ 20%) μs double exponential waves are proposed as universally sufficient inversion calculation parameters of the primary source.
4) The statistical results of the secondary side disturbance peaks of eight samples show that the disturbance level of the intelligent component acquisition port of the fusion voltage transformer under standard lightning voltage varies greatly. According to the requirements of the traditional secondary equipment EMC assessment level, there may be too strict or too loose assessment on the collection port. It is suggested to revise the relevant standards in the future.
5) The conclusions obtained in this article can fully estimate the disturbance level of the acquisition port under the lightning assessment without a high voltage level lightning impact test device. This method has relatively

low requirements for the hardware configuration of the test device, and is suitable for most manufacturers to carry out quality control according to this equivalence method.

REFERENCES

[1] S. Z. Xue, H. H. Zhao, and J. M. You, "The overview of smart grid," *Appl. Mech. Mater.*, vol. 55, no. 2, pp. 103–106, 2014.
[2] T. Yue, Z. Qin, and Y. Guoxiong, "Electromagnetic compatibility performance analysis of electronic transformers," *High Voltage Technol.*, vol. 39, no. 11, pp. 2829–2835, 2013.
[3] C. Wiggins, D. Thomas, F. Nickel, T. Salas, and S. Wright, "Transient electromagnetic interference in substations," *IEEE Trans. Power Del.*, vol. 9, no. 4, pp. 1869–1884, Oct. 1994.
[4] M. V. Matveyev, M. K. Kostin, and S. Zhivodernikov, "Some results of EMC investigations in russian substations," CIGRE, Paris, France, Tech. Rep., 2002, pp. 36–103.
[5] Z. Jun, C. Weijiang, and G. Fei, "Calculation and analysis of space magnetic field effect on intelligent components in transformer lightning impulse test," *Proc. CSEE*, vol. 36, no. 14, pp. 3981–3989, 2016.
[6] Z. Jun, C. Weijiang, and Z. Jiangong, "Calculation and analysis on electromagnetic disturbance of shielded cables in impulse test," *High Voltage Eng.*, vol. 41, no. 11, pp. 3775–3782, 2015.
[7] *Electromagnetic Compatibility—Part 4-1: Testing and Measurement Techniques-Overview of IEC 61000-4 series*, Standard IEC 61000-4-1, 2006.
[8] *Electromagnetic Compatibility—Part 4-5: Testing and Measurement Techniques-Surge Immunity Test*, Standard IEC 61000-4-5, 2014.
[9] *Low-voltage Switchgear and Controlgear Assemblies—Part 1: General*, Standard IEC 61439-1, 2011.
[10] C. E. R. Bruce and R. H. Golde, "The lightning discharge," *Inst. Elect. Eng.*, vol. 88, no. 6, pp. 487–505, Dec. 1941.
[11] F. Heidler, J. Cvetic, and B. Stanic, "Calculation of lightning current parameters," *IEEE Trans. Power Del.*, vol. 14, no. 2, pp. 399–404, Apr. 1999.
[12] M. Rubinstein and M. Uman, "Methods for calculating the electromagnetic fields from a known source distribution: Application to lightning," *IEEE Trans. Electromagn. Compat.*, vol. 31, no. 2, pp. 183–189, May 1989.
[13] *Low-Voltage Switchgear and Controlgear Assemblies—Part 1: General*, Standard IEC 61439-1, 2011.
[14] C. F. Wagner and G. D. McCann, "Induced voltages on transmission lines," *Electr. Eng.*, vol. 61, no. 12, pp. 916–929, 1942.
[15] R. Hongna, Z. Xiaoying, Z. Heng, S. Yuning, and W. Zifan, "Effect of different lightning shapes on electromagnetic spectrum characteristics," in *Proc. Asia–Pacific Int. Symp. Electromagn. Compat. (APEMC)*, May 2016, pp. 398–400.
[16] S. R. Sharma, M. Fernando, and V. Cooray, "Frequency spectrum of the electromagnetic fields of positive return strokes," in *Proc. ICLP*, 2004, pp. 80–84.
[17] A. Orlandi, C. Mazzetti, Z. Flisowski, and M. Yarmarkin, "Systematic approach for the analysis of the electromagnetic environment inside a building during lightning strike," *IEEE Trans. Electromagn. Compat.*, vol. 40, no. 4, pp. 521–535, Nov. 1998.
[18] L. Liu, X. Cui, and L. Qi, "Simulation of electromagnetic transients of the bus bar in substation by the time-domain finite-element method," *IEEE Trans. Electromagn. Compat.*, vol. 51, no. 4, pp. 1017–1025, Nov. 2009.
[19] B. Gustavsen and A. Semlyen, "Rational approximation of frequency domain responses by vector fitting," *IEEE Trans. Power Del.*, vol. 14, no. 3, pp. 1052–1061, Jul. 1999.
[20] L. Kojovic, M. Kezunovic, and C. Fromen, "A new method for the CCVT performance analysis using field measurements, signal processing and EMTP modeling," *IEEE Trans. Power Del.*, vol. 9, no. 4, pp. 1907–1915, 1994.
[21] J. He, Z. Yu, R. Zeng, B. Zhang, S. Chen, and J. Hu, "Power-frequency voltage withstand characteristics of insulations of substation secondary systems," *IEEE Trans. Power Del.*, vol. 25, no. 2, pp. 734–746, Apr. 2010.
[22] H.-T. Wu, C.-Q. Jiao, X. Cui, X.-F. Liu, and J.-F. Ji, "Transient electromagnetic disturbance induced on the ports of intelligent component of electronic instrument transformer due to switching operations in 500 kV GIS substations," *IEEE Access*, vol. 5, pp. 5104–5112, 2017.
[23] *General Technical Specification for Intelligent Overhead Pole Mounted Switch in 12 kV Distribution Network*, document T/CES 033-2019, 2019.

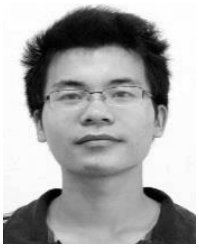

QI WANG was born in Hubei, China, in 1987. He received the B.Eng. and M.Eng. degrees in electrical engineering and automation from Wuhan University, Wuhan, China, in 2011 and 2017, respectively. He is currently pursuing the Ph.D. degree with the China Electric Power Research Institute.

He engaged in the research on the impact of strong electromagnetic transients on smart devices.

ZIHAN TENG was born in Hubei, China, in 1994. He is currently pursuing the Ph.D. degree with the China Electric Power Research Institute. He mainly engaged in the field of electromagnetic compatibility.

FANWU CHU was born in 1988. He received the Ph.D. degree from the Huazhong University of Science and Technology, Wuhan, China, in 2017. He is currently working with the China Electric Power Research Institute. His research interests are in the areas of electromagnetic calculation, monitoring, and test method of power equipment.

YUE TONG was born in Hubei, China, in 1983. She received the Ph.D. degree from the Huazhong University of Science and Technology, Wuhan, China, in 2011. She is currently working with the China Electric Power Research Institute. Her research interests include calibration of electronic current and voltage transformers and digital signal processing.

JUNJUN XIONG was born in Hubei, China, in 1987. He received the master's degree in detection technology and automatic equipment from Wuhan University, in 2012. He is currently working with the China Electric Power Research Institute. He mainly engaged in the research of electronic transformer detection technology.

GUOXIONG YE was born in Hubei, China, in 1965. He received the bachelor's and master's degrees in electrical theory and new technology from the Huazhong University of Science and Technology, in 1987 and 2002, respectively. He is currently working with the China Electric Power Research Institute, where he is also a professor-level Senior Engineer. His research interests include calibration of electronic current and voltage transformers and digital signal processing.

XIONG WU was born in Hubei, China, in 1962. He received the bachelor's and master's degrees in electric engineering from the Wuhan University of Hydraulic, Hubei, in 1984 and 1987, respectively.

He is currently a Ph.D. Supervisor with the China Electric Power Research Institute, where he is also a professor-level Senior Engineer. His research interests include electromagnetic environment, electromagnetic compatibility in power systems, power transmission, and magnetic problems in high-voltage apparatus.